J Mater Sci (2021) 56:1694–1712

Metals & corrosion

Welding thermal stress diagrams as a means of assessing material proneness to residual stresses

Andrii Mishchenko[1] and Américo Scotti[1,2,3,*]

[1] *Laprosolda-Center for Research and Development of Welding Processes, Federal University of Uberlandia (UFU), Uberlândia, MG, Brazil*

[2] *Division of Welding Technology, Department of Engineering Science, Production Technology West, University West, Trollhättan, Sweden*

[3] *Graduate Program in Materials Science and Engineering, Federal University of Parana (UFPR), Curitiba, PR, Brazil*

Received: 19 May 2020
Accepted: 22 August 2020
Published online: 21 September 2020

ABSTRACT

In this work, the proposal and appraisal of a method to describe in a quantitative manner the phenomenon of thermal stresses formation in welding at different heat-affected zone (HAZ) regions and under different cooling rates, by means of physical simulation, are explained. Under the denomination of welding thermal stress diagrams (WTSD), initially the concept and experimental arrangements needed to use the idea, based on a Gleeble simulator, are revealed. An approach to determine more realistic thermal cycles (peak temperature and heating/cooling rates) is introduced and applied. The method assessment was carried out by using specimens of a HSLA quenchable steel subjected to different cooling rates (covering a wide range of typical welding heat inputs) and peak temperatures (representing regions progressively farther away from the fusion line). The different thermal stress (TS) curves proved the concept based on the justification of the results. In addition, it was physically demonstrated that TS curves are governed mainly by two complex concurrent phenomena, namely contraction under restriction of heated areas and the expansibility of phase transformation. It was concluded that due to this balance, the highest residual stress (RS) does not occur either at slowest cooling rate or at fastest cooling rate. Nevertheless, the highest RS may not occur at the coarse grain zone either. TS progressively drops along the HAZ regions away from critical regions, and even at sub-critical regions there is tensile RS. Complementarily, it was also concluded that WTSD by physical simulation allows one to determine the deformation behaviour of a material as a function of temperature. This information can be used as input or calibration in modelling for thermal stress generation in steels.

Handling Editor: Nathan Mara.

Address correspondence to E-mail: americo.scotti@hv.se; ascotti@ufu.br

https://doi.org/10.1007/s10853-020-05294-y

Introduction

Heat input physical simulation in welding is achievable by submitting a material to typical welding thermal cycles. Thereafter, the metallurgical response of this material under these thermal cycles is reached without doing actual welding. Traditionally, physical simulations of welding focus on studying the influence of thermal cycle operational parameters (heating and cooling rates and peak temperature) on the microstructure and mechanical properties (hardness and impact resistance, mainly) of the heat-affected zone (HAZ). As an example, Shome and Mohanty [1] developed continuous cooling transformation (CCT) diagrams for high-strength low-alloy (HSLA) steels, simulating welding within a range of heat inputs and at different peak temperatures (covering the coarse grain and refined grain regions). Cruz-Crespo et al. [2] simulated tempering passes applied to a HSLA steel and studied consequent retreated HAZ microstructures. Scotti et al. [3]. demonstrated, on the other hand, a need for harmonized procedures and microconstituent terminologies through a Round Robin test on thermal simulation to draw repeatable CCT diagrams.

However, another welding physical simulation application, although much less popular, would be studying thermal stresses (TS) generated in a material during welding. It is worthy to mention that thermal stresses importance is often overlooked when the purpose is to evaluate residual stresses (RS). However, this practice does not seem coherent, because TS precedes RS and, consequently, TS is fundamental in understanding the RS final state. In this sense, Jones et al. [4] have already physically simulated the TS in non-alloyed and alloyed carbon and stainless steels. To reproduce the restraint which might be expected in welded joints, unloaded specimens were first heated to the peak temperature of 1320 °C and, then, maintained at a constant length during cooling. The contraction-related load required to maintain this length was continuously monitored, corresponding to the TS generated. Although observing the TS only during cooling, as shown in Fig. 1, the data obtained by Jones and co-workers indicated behaviour similarities to materials under restraint and cooling. The transient inversion of the trends of increasing stress as the material cools down (due to contraction), which happens in Fig. 1 from 600 to 200 °C,

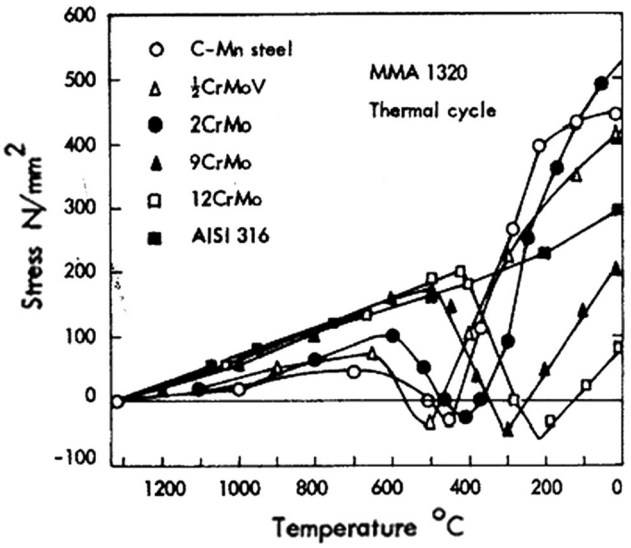

Figure 1 Profile of thermal stresses (TS) generated during cooling in physical simulation (using a weld simulator named MMA-1320 and a thermal cycle similar to that experienced by HAZ during manual metal arc welding) and resulting residual stresses (RS), from various steels under the same restraints and welding thermal cycles (after Jones et al. [4]).

characterizes phase transformation of expansive character. The final values of TS at room temperature correspond to RS. As can be seen, the materials that undergo martensitic transformation during cooling (9CrMo and 12CrMo) at lower temperatures presented lower RS. On the other hand, austenitic steel AISI 316 that does not go through transformations in solid state has an intermediate RS value, between materials that have high martensitic transformation temperature and those that have low. These observations indicate, for instance, the potential that physical simulations present for the study of LTT (low-temperature transformation) steels and prediction of their impact on resultant RS.

It is important to mention that Jones et al. [4] measured TS accumulated due to contraction and affected by phase transformation under a single cooling rate. Therefore, potential effect of heat input was not considered. Scotti [5], in turn, presented descriptive models aiming at understanding the heat input (and corresponding cooling rates) effect on TS. Contraction is greater for higher heat input, which favours larger volume heated but also for uneven temperature along the heated material. Phase transformation expansion intensity depends on the material (composition and thermomechanical history) and on the experimented cooling rate. Scotti's models

claim to explain the reason for a non-proportional decay of RS from weld centre line towards non-heated material.

However, for some reason or other, the thermal cycle of a real welding in physical simulation studies is not always faithfully represented and some thermal cycle parameters are sometimes neglected, such as heating rate and peak temperatures. As stated by Poorhaydari et al. [6], a typical arc weld thermal cycle consists of very rapid heating (several hundreds of degrees per second) to a peak temperature, followed by relatively fast cooling (a few tens or hundreds of degrees per second) to ambient temperature. Kumar et al. [7] showed that there is a relationship between welding energy and heating rate; the higher the welding energy, the slower the heating rate. Notwithstanding, some researchers have not paid attention to this relationship. Xu et al. [8] studied the effect of heat imposed on the properties of simulated HAZ in high-strength microalloyed steels and heated the samples at a fixed rate of 100 °C s^{-1}, regardless of the cooling rates used. Similarly, Wang et al. [9] simulated the HAZ microstructures of a X80 steel by heating the sample at a faster fixed rate of 160 °C s^{-1} and up to only 1250 °C. Jordan et al. [10] through physical simulation studied the effect of welding on the microstructure of ferrous alloys and heated the sample only up to 1200 °C, but in a much faster fixed heating rate of 1000 °C s^{-1}. There are other divergences between welding thermal cycles applied in physical simulations and actual thermal cycles. The existence of a pause time at the peak temperature is one of them. For example, Ramirez et al. [11] studied primary and secondary intragranular austenite precipitation and its relationship with chromium nitrite (Cr_2N) in simulated HAZ of multipass welding of duplex stainless steels. The authors chose to represent the HAZ of a weld 1350 °C as peak temperature, but with a pause of 5 to 10 s at this level and a rapid cooling up to room temperature.

Other researchers were concerned about obtaining more realistic thermal cycles, function of the operational parameters (current, voltage and welding speed), by using Rosenthal [12] or Rykalin [13] equations under different conditions. Hattingh and Pienaar [14] studied the effect of Nb on the HAZ mechanical properties by means of Rosenthal's equations to simulate thermal cycles under distinct heat inputs. Moon et al. [15] also used Rosenthal's equations to calculate the thermal cycle to simulate the HAZ coarse region of HSLA steels. Kumar et al. [16], in turn, used Rykalin equations to calculate thermal welding cycles to be simulated in thick plate of a high-strength microalloyed steel, and Zheng et al. [17] used the same equations to simulate thermal cycles equivalent to welding with several energies.

As seen above, there is still a lack of a systematic methodology and validation thereof to have physical simulation applied to assess material proneness to residual stresses. To overcome this drawback encouraged the authors of the current work to propose a method to describe quantitatively the phenomenon of thermal stresses formation in a real welding situation, and this has great potential for the study of thermal and residual stresses. The concept of this method was denominated welding thermal stress diagrams (see "The concept of a welding thermal stress diagram" section). Therefore, the present study aims at proposing a methodology for raising welding thermal stress diagrams (WTSD) and for studying thermal stress evolution and residual stress, including a determination approach of thermal cycles that reproduces actual welding conditions.

The concept of a welding thermal stress diagram

Similar to the approach of Jones et al. [4], WTSD is raised by heat input physical simulation, where a specimen taken from the base metal (BM) under investigation and of predefined geometry is subjected to a thermal cycle (heating rate, peak temperature and cooling rate) typical of welding. If the specimen remains restricted (constant displacement between specimen holders) during heating and cooling and the reaction forces exerted by the specimens on the holder are measured by a load cell, it is possible to calculate the stress along time and obtain curves that demonstrate temporal evolution of the thermal stresses generated, as schematized in Fig. 2. It is well known that, if the material is under different heat inputs, the imposed thermal cycles will diverse, characterizing dissimilar regions of HAZ (size and heating/cooling rates).

One can observe in Fig. 2 that during the heating stage the specimen is under compressive stress, due to restriction of the thermal expansion. The intensities of compressive stresses depend, for a given material,

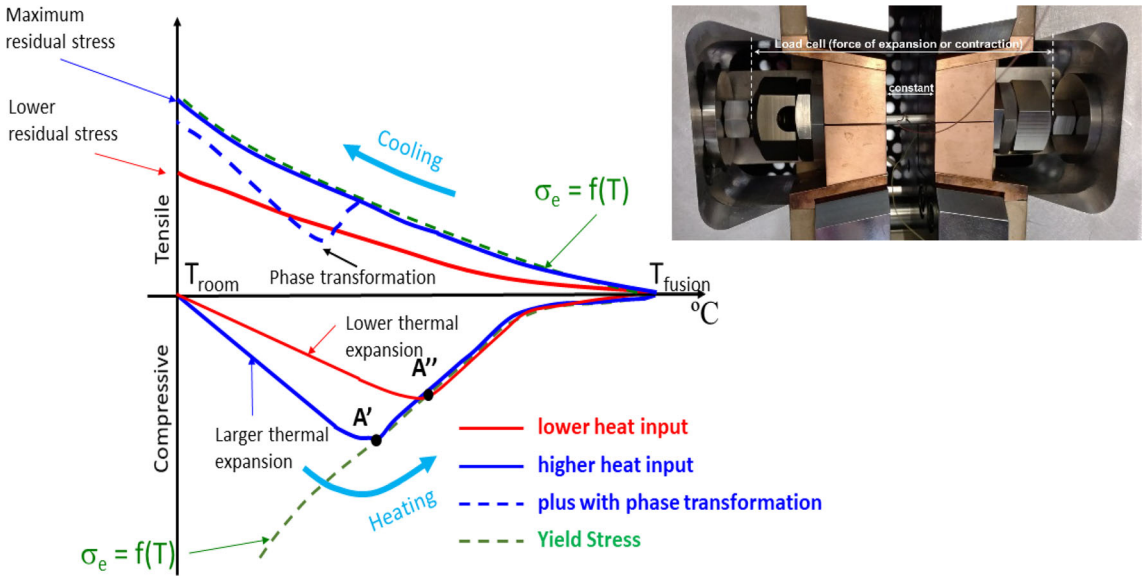

Figure 2 Schematic representation of a WTSD (welding thermal stress diagram), where σ_e is the yield stress resistance of the material (this representation shows cases of a same hypothetical material—same yield stresses—under different heat inputs and material under higher heat input with and without phase transformation during cooling).

on the heated volume. (Greater volume causes more expansion at a similar temperature difference.) As material yield stress (σ_e) decreases with increasing temperatures (green line in compressive stress side of the diagram), the compressive stress (in elastic regime), which increases with temperature (restricted expansion), will, at a certain temperature value, match that of the material at this temperature. As the material undergoes plastic deformation when worked at the yield stress, the value of compressive stress begins to be reduced with the increase in temperature, even if thermal dilatation tended to be higher (red, blue and green lines, Fig. 2, after meeting each other). In theory, stress is nil when melting point is reached, since the pool would no longer offer any constraint.

Nevertheless, specimen behaviour changes when there is variation in the volume of the heated metal, as happens in a weld bead made with higher welding energies; the volume of heated metal is larger, resulting in greater expansion and, consequently, higher TS for a given heating temperature (blue line in compressive stress side of Fig. 2). On the other hand, a weld bead made with lower energy has smaller heated metal volume, leading to lower expansion and lower TS (red line in compressive stress side of Fig. 2). Thus, temperatures and intensities in which compressive stress is equal to those of yield stress are different, according to welding energy (which governs heat input). Therefore, once the yield stress resistance is reached, consequently entering plastic regime, stress is the same for a given material as the temperature continues to grow (red, blue and green lines, in Fig. 2, after they have met each other).

In the cooling phase, material that had greater thermal expansion due to higher heat input (larger heated volume) will also generate greater thermal contraction, that is, greater contraction stresses, which, because they have restricted movement, generate tensile stresses in the material. As yield stress increases as temperature drops (the ability of material to absorb deformation decreases), maximum intensity of tensile stress reached by a material is increasing with a reduction in temperature. (Intensity of stress is never higher than yield stress, because if σ exceeds σ_e, the material undergoes plastic deformation.) Therefore, if material has had a large volume heated, consequently large contraction (blue line in cooling phase of Fig. 2), the stress at the end of cooling (residual stress) will be the same as the yield stress at room temperature. However, if contraction is smaller (red line in cooling phase of Fig. 2), the intensity of tensile stress, in elastic regime, does not reach yield stress, and residual stress will be lower.

Finally, the presence of phase transformations may concomitantly be manifested by the tensile stress curve during cooling. Because transformations are

expansive, they reduce the intensity of the tensile stresses at temperatures in which transformations take place (blue line dashed in cooling phase of Fig. 2). As a result, the final tensile stress (room temperature), i.e. residual stress, can become lower than when the material presents no transformation. And, the lower the temperature that this transformation takes place, the lower the final value (principle of LTT material, described, for instance, by Çam et al. [18] and Kannengiesser and Kromm [19]).

Simulator set-up and specimen geometry and dimension to raise WTSD

A Gleeble® thermal–mechanical simulator (model 3550-GTC) was used in this work to keep the specimens restricted during controlled heating and cooling and to have reaction forces exerted by the specimens on the holder measured by a load cell. Figure 3 illustrates the experimental assembly. The under-study metal specimen (1) is fixed between the copper jaws (2), which, by being water-cooled, can cool the specimen down quickly by heat conduction. By means of a set of nuts (3), the specimen is rigidly attached to the jaws, with no freedom of movement, while the piston (4) ensures positioning of specimen to reach null load condition at start, as well as to prevent any subsequent movement of specimen holder. During heating and cooling, the efforts due to expansion and contraction of the specimen on the jaws are perceived by a sensor (L-gauge), not visible in this figure. Specimen temperature is measured by a very thin thermocouple, usually of type "K" (function of desired thermal cycle), fixed at the centre of specimen and connected to port (5). The temperature measured is what allows for the control of specimen heating and cooling cycles, by continuous comparison of value measured by thermocouple with a value defined by user in script. Scripts are user-filled tables that contain sequential instructions for the equipment, basically initial heating/cooling temperature, final heating/cooling temperature and their times in temperature ranges, plus other information for equipment set-up.

In relation to specimen geometry, a cylindrical bar (easily machined) with threaded ends (to avoid slipping at jaws) would be the ideal shape. In theory, the larger the bar diameter, the more sensitive would be the output (reaction forces as a function of temperature). Nonetheless, this geometry and dimension present some drawbacks when Gleeble is used. The first one is related to Joule heating, making it difficult to reach very fast heating times, typical of welding. The second issue is related to maximum clearance between the two jaws, increasing the likelihood of having full specimen heated between the two jaws, regardless of simulated value of welding energy. If the full length of specimen is always heated, the effect of heat input in thermal stress generation cannot be quantified. To minimize these drawbacks, even at the expense of reduced sensibility, the proposed specimens used in this work had geometry and dimension as presented in Fig. 4.

To make the physical simulation even more efficient, vacuum was replaced by forced air inside the Gleeble chamber, making faster cooling rates possible. A setback of this approach was reduced temperature homogeneity at the central cross section of the specimens, a problem that showed itself to be not

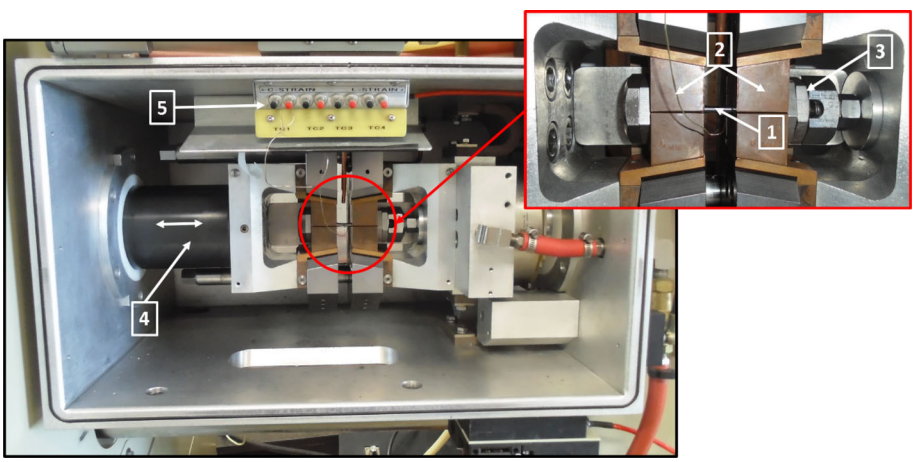

Figure 3 Experimental assembly to raise WTSD by using a Gleeble® Thermal–Mechanical Simulator (model 3550-GTC): 1 = specimen; 2 = water-cooled jaws (2); 3 = nuts to load and unload specimens (3 × 2); 4 = hydraulic system to position jaws; 5 = thermocouple port.

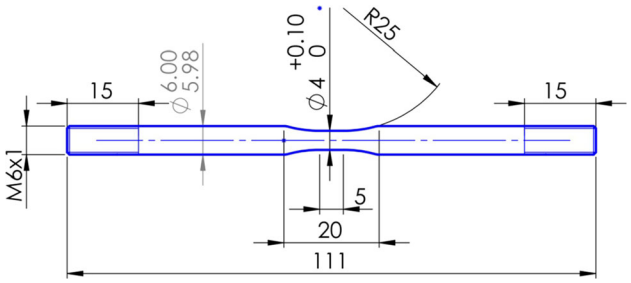

Figure 4 Specimens designed with reduced cross section at centre.

so critical because of small diameter of central part. With all of these expedients, heating rate up to 1000 °C s^{-1} from 600 °C to 1350 °C and cooling rates up to 135 °C s^{-1} from 800 to 500 °C were reached, making it possible to perform all predicted tests.

Thermal cycle parameterization and script

Basically, the above-mentioned scripts are sequential instructions for the equipment to perform the thermal cycles. To predict thermal cycles is not a simple task. Several authors have developed and demonstrated analytical solutions for this purpose, but with simplifications. The most famous solutions were presented by Rosenthal [12], in which limitations are grounded mainly on the assumption of a moving point heat source on a plate surface (neglecting any heat transfer from surface), on which physical coefficients were independent of temperature and on the fact that all energy from welding equipment was transferred to arc, as summarized in Poorhaydari et al. [6]. In addition, Rosenthal's equations to predict weld thermal history were developed to a bead-on-plate condition (not taking into account groove effect). Numerical solutions are likely more precise by better managing the material shape and properties, but these approaches are very time-consuming and computer resource consuming. In addition, different real welds are unique in relation to thermal history. Even a single thermal cycle is different at different regions of the same weld bead (for instance, comparing bottom and near-surface positions). As shown, to be inclined towards a more precise approach will not overcome all setbacks. Therefore, the proposed thermal cycle parameterization in this work aims at trends and not quantities.

Rosenthal's equations are well known and easily found in several bibliographic sources. Therefore, due to lack of space, they will not be presented in this work. In fact, Rosenthal proposed two sets of solutions in his questioning. One set was derived for thick plates (assuming 3-D heat flow) and the other for thin plates (assuming 2-D heat flow). There is also an equation to determine a critical thickness for a given heat input at which the 2-D condition prevails. However, there is a confounding gap of thickness to which neither 2-D nor 3-D is applied. Poorhaydari et al. [6] cite that the most actual conditions lie somewhere in between the two extremes. Aiming at sorting out this problem, Poorhaydari et al. proposed a weighting factor to Rosenthal's analytical solutions for cooling rate calculations of welding on thick and thin plates. The factor is determined from HAZ width, obtained from etched sections, which reflects the actual response of the plate to heat flow conditions.

By using Rosenthal's equations, and if needed Poorhaydari et al.'s corrective factor, simulated temperature as a function of time curves resultant from a given parameterization is determined. These temperatures × times represent the full thermal cycles (heating and cooling rates and peak temperature) at a desirable position in the heat-affected zone (HAZ) of a given weld bead (plate material and thickness and arc energy). The procedure applied to determine these actual welding thermal cycles is summarized as follows (more details can be found at Mishchenko [20]):

(a) Input parameters are the distance from a desired position at HAZ to the heat source centreline (r), heat input (q/v), base material thickness (d) and properties, initial temperature of plate (T_0) and peak temperature (T_p) and cooling time from 800° to 500 °C ($\Delta t_{8\text{-}5}$);
(b) A suggestion to minimize limitations of Rosenthal's equations is to measure distance from desired position to heat source centreline (r) from a cross section of an actual weld over a plate with the same material and thickness as that of the material under investigation for thermal stress generation;
(c) Heat input is generally estimated by ratio of average instantaneous arc power (q) and travel speed (v) (see remarks on methods and limitations of arc power calculations in Jorge et al.

[21]) multiplied by a thermal efficiency factor (η_t). However, intrinsic errors and difficulties to measure thermal efficiency have been demonstrated by Liskevych and Scotti [22] and Hurtig et al. [23]. For this reason, and considering the use of resultant actual weld cross sections, in this work the heat input-related input parameter used in Rosenthal's equations is replaced by arc energy (q/v);

(d) With the input parameters, the heating and cooling times and peak temperature profiles are traced for each desirable condition;

(e) In order to facilitate script programming on Gleeble, the thermal cycle generated is discretized in linear stretches, as illustrated in Fig. 5.

Assessment of welding thermal stress diagram concept

Experimental set-up

Using a quenchable high-strength low-alloy (HSLA) steel as reference (see Table 1), different WTSDs were raised using different cooling rates (10, 30, 50, 55, 75, 90, 100 °C s^{-1}) and four peak temperatures (T_{peak} = 1350 °C, 1100 °C, 900 °C and 700 °C). The different peak temperatures represent heat-affected zone (HAZ) regions progressively farther away from fusion line, i.e. T_{peak} = 1350 °C would represent a region of HAZ with coarse grains, while samples with T_{peak} of 1100 °C a region of fine grains, samples with T_{peak} of 900 °C a intercritical region and samples with T_{peak} of 700 °C a subcritical region. The reason for studying different regions is that one would expect different thermal stress (TS) generation at diverse HAZ regions of a weld (thermal expansion and metallurgical transformation). Scanning of the cooling rates is justified because metallurgical transformation is one of the governing factors of TS generation.

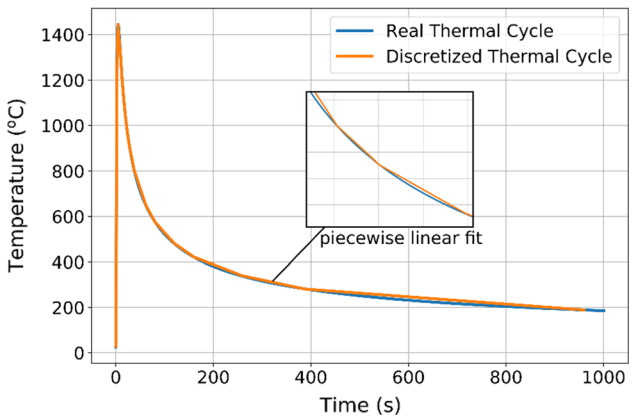

Figure 5 Linear discretization scheme of thermal cycle generated through Rosenthal's equations.

Table 1 Measured properties of the HSLA steel used to raise WTSD

C	Si	Mn	P	S	Al
0.12	0.07	1.73	0.023	0.003	0.042

Material provided in plates of 300 × 250 × 6.35 mm, constituted of ferritic–bainitic microstructure, YS = 758 MPa, UT = 861 MPa and microhardness of 259 HV ± 11 HV

Table 2 summarizes values calculated according to the procedure described in Sect. 4, and consequently programmed for use on Gleeble, and values measured after simulation. It is important to mention that cooling rates ($CR_{8\text{-}5}$) were accompanied by respective heat rates ($HR_{6\text{-}Tp}$). They were calculated with the aid of Rosenthal's 2D equations, considering a plate with 6.35 mm. (This plate thickness was subjectively chosen, based on the material provided for the test.)

Simulation results were analysed according to the parameters obtained from WTSD curves (see Fig. 6), namely starting and finishing temperatures of cooling phase transformation (FTT), inclination of stress–temperature curves ($d\sigma/dT$) before and after phase transformation, thermal stress values before and after phase transformations (TS_s and TS_f, respectively) and final residual stress value (RS). It is noteworthy that the slopes of stress–temperature curves after phase transformation have a special meaning, corresponding to the hardening or not of material after phase transformation. These parameters were determined by dedicated software developed in MathLab.

The length of heated metal volume was also measured in each specimen, from video-recorded images during each test. The video was discretized in frames, and then a visual analysis of the entire heating and cooling period was performed in order to detect the moment when the visible heated region was at its longest possible length.

Microstructural analysis was finally performed on 4-mm-diameter cross sections taken from the centre

Table 2 Heating rates ($HR_{6\text{-}Tp}$) and cooling rates ($CR_{8\text{-}5}$) for different peak temperatures

T_{peak} (°C)	$HR_{6\text{-}Tp}$ (°C s^{-1}) programmed (measured)	$CR_{8\text{-}5}$(°C s^{-1}) programmed (measured)
1350	109 (110.09)	10 (10.02)
	329 (330.03)	30 (29.96)
	548 (550.23)	50 (53.32)
	603 (605.99)	55 (54.99)
	822 (833.01)	75 (78.86)
	987 (962.21)	90 (90.81)
	1096 (1046.55)	100 (101.30)
1100	206 (208.05)	30 (30.00)
	377 (385.56)	55 (55.16)
	617 (625.52)	90 (89.51)
900	107 (112.57)	30 (29.95)
	321 (322.90)	90 (89.54)
700	76 (76.79)	30 (33.27)
	228 (228.96)	90 (97.85)

T_{peak} = peak temperature; $HR_{6\text{-}Tp}$ = heating rate from 600 to programmed peak temperature; $CR_{8\text{-}5}$ = cooling rate from 800 to 500 °C

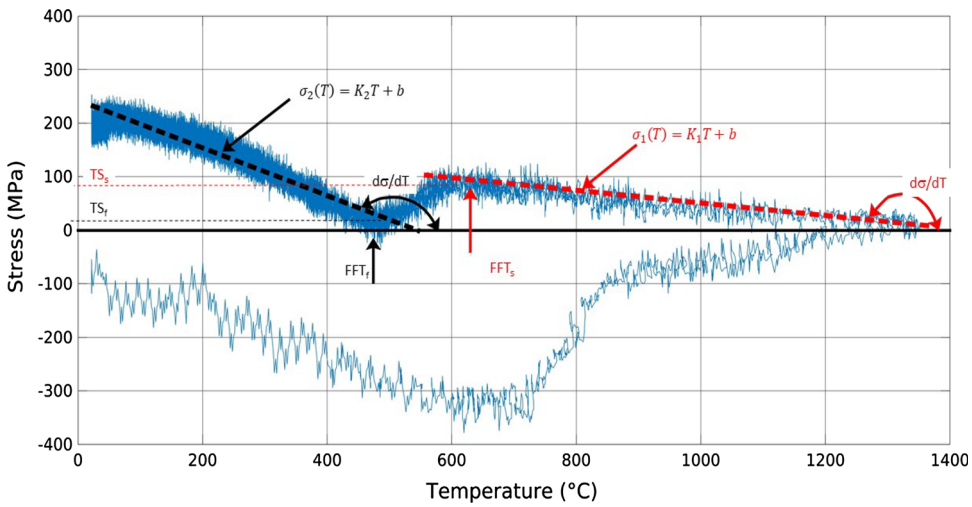

Figure 6 Schematization of parameters obtained from WTSD curves: starting temperature (FTT_s) and finishing temperature (FTT_f) of phase transformation during cooling; slope of stress–temperature curves ($d\sigma/dT$) before and after phase transformation; thermal stress values before (TS_s) and after (TS_f) phase transformations; residual stress value (RS).

of the specimen, where the thermocouples were welded. In addition, a HV microhardness profile (500 g load and 15 s straightener retention time) was taken in the middle of the cross section, with a 0.25-mm space between each indentation, totalling 14 measurements. (One measurement was discarded at the beginning and end of the measurement line, being were very close to the edge.)

Results and discussion

Thermal cycles with T_{peak} of 1350 °C

Figure 7 presents the WTSD for peak temperature of 1350 °C. This temperature would represent a coarse grain region of a heat-affected zone (CG-HAZ) of the steel under study. Several aspects can be observed in relation to influence of heating/cooling rates on material behaviour. The first aspect to draw one's attention is maximum temperature reached during heating for the 2 fastest $CR_{8\text{-}5}$, which are slightly higher than for other rates, yet the stress to reach the YS is significantly lower. One must realize that $CR_{8\text{-}5}$ would not influence the heating stage, but on the other hand, the faster the $CR_{8\text{-}5}$, proportionally faster is the heating rate from 600 °C to programmed peak temperature ($HR_{6\text{-}Tp}$) to simulate actual welding (see Table 2). From a faster $HR_{6\text{-}Tp}$, one can expect a higher austenization starting temperature and shorter time during heating above the austenization temperature (fine austenite grain size). There is,

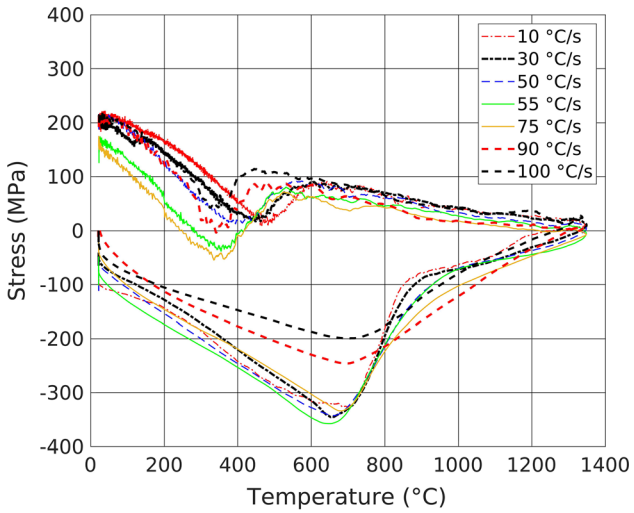

Figure 7 WTSD for different cooling/heating rates having a peak temperature of 1350 °C.

therefore, no clear relationship between these facts and lower YS. The likely explanation for this phenomenon is a dynamic response limitation of the stress sensor (L-gauge), not being able to capture changes at the same speed as that of the phenomenon. (In fact, this anomaly occurred only with these two cases and the higher temperatures for reaching YS are strong evidence to support this observation.) In other words, the phenomenon is correct, yet the test monitoring is faulty for such a high heating rate. Fortunately, this test limitation does not impact cooling cycles, which have much slower rates than those of heating rates.

A second aspect to draw attention to is that for heating rates from 10 to 75 °C s^{-1}. A YS of around 680 °C is reached when plastic deformation/phase transformation takes place and the TS drops. The slope of the TS drop is reduced at around 900 °C, suggesting another phase transformation. Very little influence of heating rate is detected, considering the intrinsic inaccuracy expected for sensor and signal deviations from an average.

Having said this, the analysis will concentrate now on cooling cycles. As observed in Fig. 8a, starting and finishing transformation temperatures are inversely proportional to $CR_{8\text{-}5}$. This fact would be justifiable from the metallurgical point of view, since with an increase in the cooling rate, the degree of supercooling increases and atomic diffusion speed decreases, which causes phase transformations to occur at lower temperatures. Zhao et al. [24], who, through physical simulations, studied the effect of the cooling rate (from 0.5 to 8 °C s^{-1}) on phase transformation and microstructure of a NbTi microalloyed steel with chemical composition similar to the steel under study, found the same trend. Figure 8b shows that it was not only transformation temperatures that changed with increasing $CR_{8\text{-}5}$, but also stresses accumulated when these transformations took place. It can be observed in Fig. 8c that the slope of the stress–temperature curve ($d\sigma/dT$) before phase transformation is not influenced by the thermal cycle, a fact justified by the behaviour of the common austenitic microstructures. The stress–temperature curve ($d\sigma/dT$) after phase transformation, in turn, evidenced the effect of microstructures (type, grain size and hardness); steeper slopes occurred for CR8-5 measured from 53.32 to 78.86 °C s^{-1}.

Micrographics of cross sections and respective average values of microhardness are shown in Fig. 9. Except for the lowest $CR_{8\text{-}5}$ (10 °C s^{-1}), hardness values are high, corroborating the appearance of a predominant presence of martensite and bainite. These morphologies are in accordance with the CCT diagram of the steel under study, as shown in Fig. 10.

Figure 11b shows the residual stresses (RS) after cooling of all specimens. It is important to recall that RS is a resultant from both the under-restriction contraction of heated material and the behaviour of microconstituents during cooling (deformability under compressive load and expansibility during phase transformation). As shown in Fig. 11a, the length of heated metal volume was, as expected, inversely proportional to $CR_{8\text{-}5}$, that is, lower energy, faster $CR_{8\text{-}5}$. Thus, in this regard, a fast $CR_{8\text{-}5}$ would lead to lower residual stress at room temperature (RS). Concerning microstructure deformability, TS fully reached to all the cases the steel YS during most of the time of the cooling phase (up to beginning temperature of the phase transformation during cooling). Finally, $d\sigma/dT$ after phase transformation alone did not define the RS, because thermal stresses at the finishing transformation temperature are highly dependent on material and $CR_{8\text{-}5}$ (Fig. 8b).

Due to a combination of factors, $CR_{8\text{-}5}$ of 55 and 75 °C s^{-1}, despite the highest $d\sigma/dT$ after phase transformation (Fig. 8c) and not the shortest heated length at the specimen centre (Fig. 11a), presented a minimal TS after transformation (more expansive transformation, actually, reaching compressive stresses—Fig. 8b), as shown in Fig. 11b. It could be

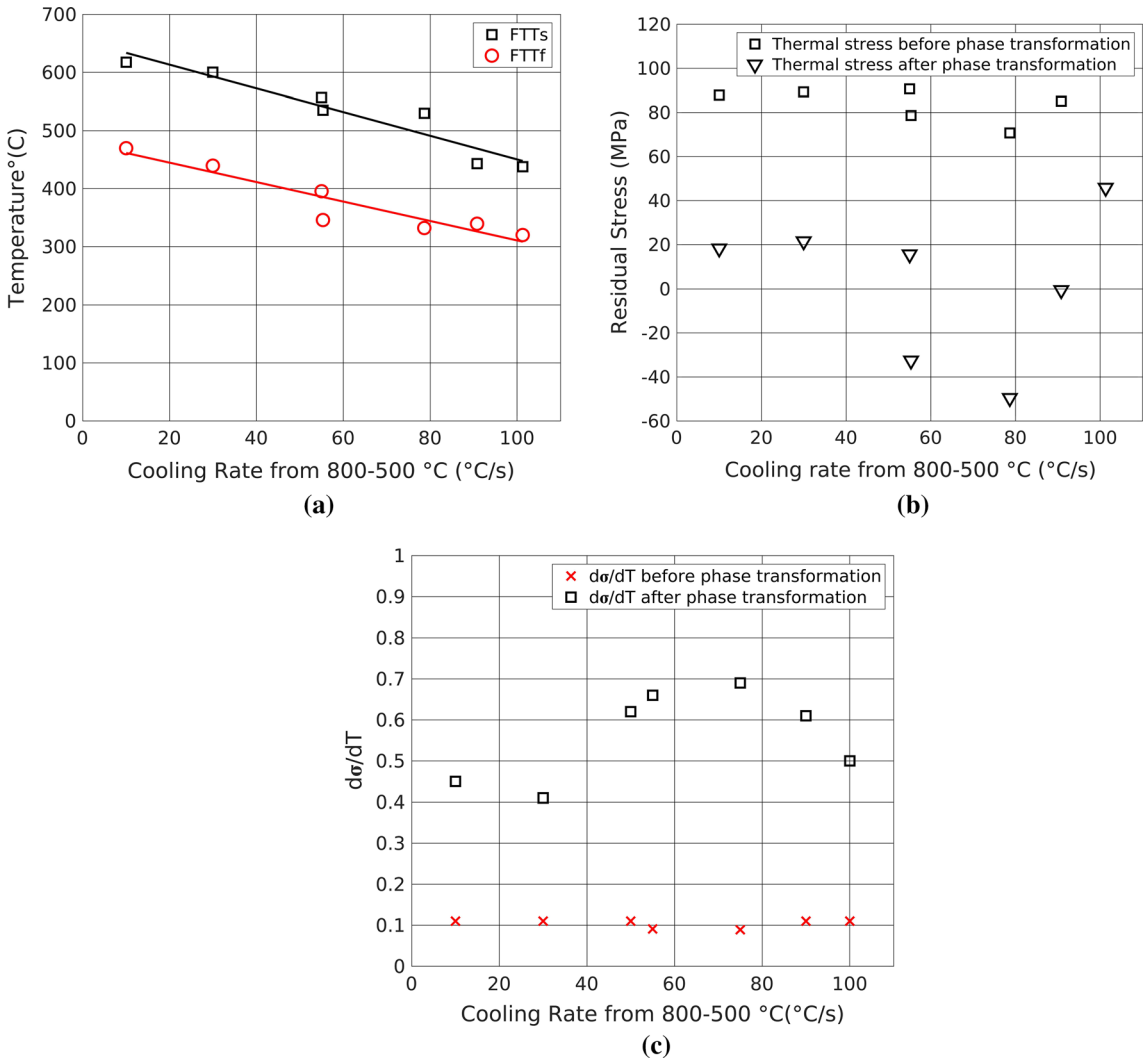

Figure 8 WTSD parameters (Fig. 6) as a function of cooling rate (measured values) for peak temperature of 1350 °C: **a** starting (FTT_s) and finishing (FTT_f) phase transformation temperatures; **b** thermal stresses before and after phase transformation during cooling; **c** stress–temperature curve slope ($d\sigma/dT$) before and after phase transformation.

argued whether the highest $CR_{8\text{-}5}$ (90 and 100 °C s^{-1}) should not have transformed into more expansive constituents or not. To debate this argument, the role of the fastest heating rate ($HR_{6\text{-}Tp}$) is uncovered. Finer grains (differences not so easily perceived by optical microscope) are expected if compared with intermediate $CR_{8\text{-}5}$ and $HR_{6\text{-}Tp}$, reducing quenchability of the material. It is important to mention that, regardless of $CR_{8\text{-}5}$ and $HR_{6\text{-}Tp}$, RS was far below the YS of the steel (Table 1), i.e. RS is in the elastic regime.

Therefore, for the HSLA steel under study, which presents high quenchability, the effect of expansibility during phase transformation showed itself to prevail over the under-restriction contraction of heated material on RS generation. In fact, for $CR_{8\text{-}5}$ from 55 to 75 °C s^{-1} this material worked as a low-temperature transformation (LTT) material.

Thermal cycles with T_{peak} of 1100 °C

Peak temperature of 1100 °C would represent a refined grain region of a heat-affected zone (FG-HAZ) of the steel under study. As planned in Table 2, for this T_{peak} only 3 nominal values of $CR_{8\text{-}5}$ (30, 55 and 90 °C s^{-1}) were assessed. Figure 12 presents the WTSD for this peak temperature. By comparing Fig. 12 with Fig. 6 (T_{peak} of 1350 °C), one can initially see that starting transformation temperatures during heating are slighter higher and stresses at transformation temperature are lower. Although this is

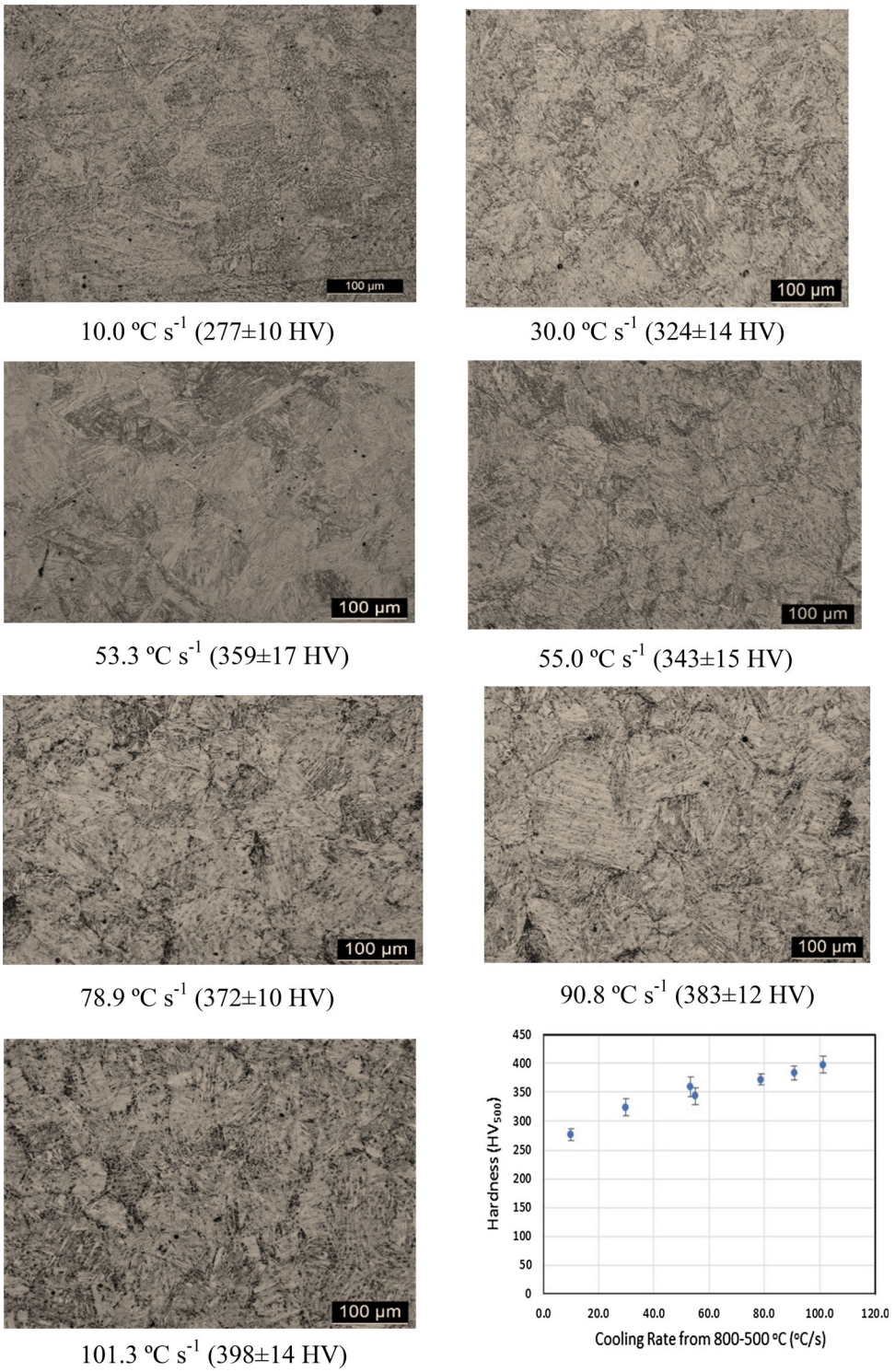

Figure 9 Microstructures of cross sections and respective average hardness (HV_{500}) of simulated specimens as a function of cooling rate (measured values) for peak temperature of 1350 °C.

unexpected behaviour at first sight, one must observe in Table 2 that the corresponding $HR_{6\text{-}Tp}$ values were significantly lower (as predicted from actual welding). This means longer heating times, favouring a late temperature transformation and offering less resistance to metal expansion. For the same reason (lower $HR_{6\text{-}Tp}$), no different behaviour of heating curve for 90 °C s^{-1} was observed, therefore supporting the justification already given for the case of T_{peak} equal to 1350 °C.

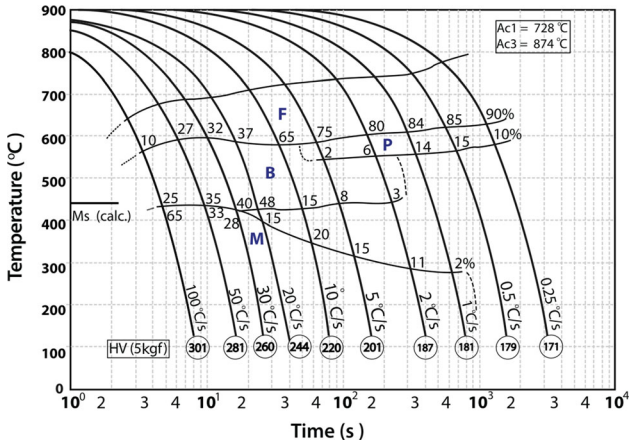

Figure 10 CCT diagram of the HSLA steel (Table 1).

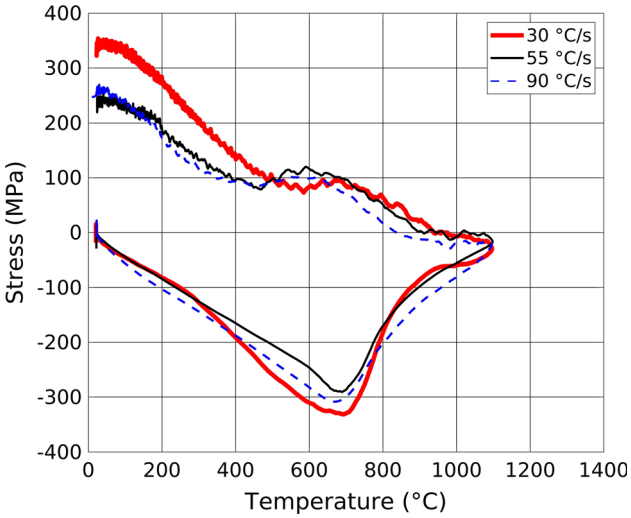

Figure 12 WTSD for different cooling/heating rates having a peak temperature of 1100 °C.

Another visible difference from comparing both figures was the starting and finishing transformation temperatures during cooling, which occurred at higher temperatures. As mentioned, the transformation expected during heating would lead to fine grains, with low quenchability. Therefore, phase transformation could start at higher temperatures. (Transformation curves of Fig. 10 would move up.)

As observed in Fig. 13, starting and finishing transformation temperatures are also inversely proportional to $CR_{8\text{-}5}$, although the effect of $CR_{8\text{-}5}$ is less than when T_{peak} was 1350 °C (see Fig. 8a). Similar to T_{peak} of 1350 °C case, the slope of the stress–temperature curve ($d\sigma/dT$) before phase transformation is not influenced by the thermal cycle, although in this case the stress–temperature curve after phase transformation does not present a clear trend.

Micrographics of cross sections and respective average values of microhardness are shown in Fig. 14. A predominance of martensite and bainite seems to occur only for the highest value of $CR_{8\text{-}5}$. Hardness values of conditions with slower $CR_{8\text{-}5}$ are only slightly higher than base metal hardness (Table 1).

As video image contrast was not good enough when a T_{peak} of 1100 °C was the target, measurements of length of heated metal volume were not possible from recorded images. Therefore, the effect

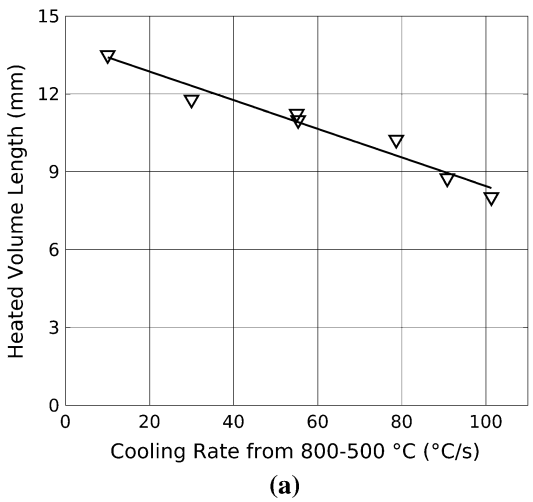

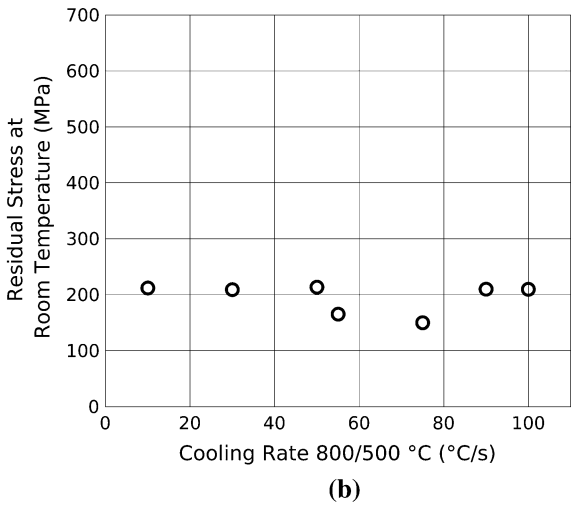

Figure 11 Residual stress-related WTSD parameters (Fig. 6) as a function of cooling rate (measured values) for peak temperature of 1350 °C: **a** visible heated volume length at specimen centre during tests (measured as proposed in "Experimental set-up" section); **b** thermal stress at room temperature after cooling (representing residual stresses).

of under-restriction contraction on RS generation was not quantified. However, Fig. 15 shows that, by comparing with the case using T_{peak} of 1350 °C (Fig. 11b), residual stresses (RS) were much lower in the specimen with T_{peak} of 1350 °C. As shown in Fig. 12, the effect of expansibility during phase transformation seems to be very small, showing under-restriction contraction of heated material on RS generation to prevail. (The slower the $CR_{8\text{-}5}$, equivalent to higher heat input, the higher the RS.) This fact justifies the highest RS at this peak temperature.

Thermal cycles with T_{peak} of 900 °C and T_{peak} of 700 °C

Peak temperature of 900 °C would represent an intercritical region of a heat-affected zone (IC-HAZ) of the steel under study, while peak temperature of 700 °C would represent a subcritical region of a heat-affected zone (IC-HAZ) of the same steel. It had not been found in the literature the A3 and the A1 lines of the steel under study. Based on a pure Fe–C equilibrium diagram, the A3 temperature would be around 910 °C, while A1 temperature would lay around 727 °C. One can assume that, if on the one hand increase in C and presence of Mn and Si would shift down these temperatures (mainly A3), on the other hand fast heating rate would make an upward

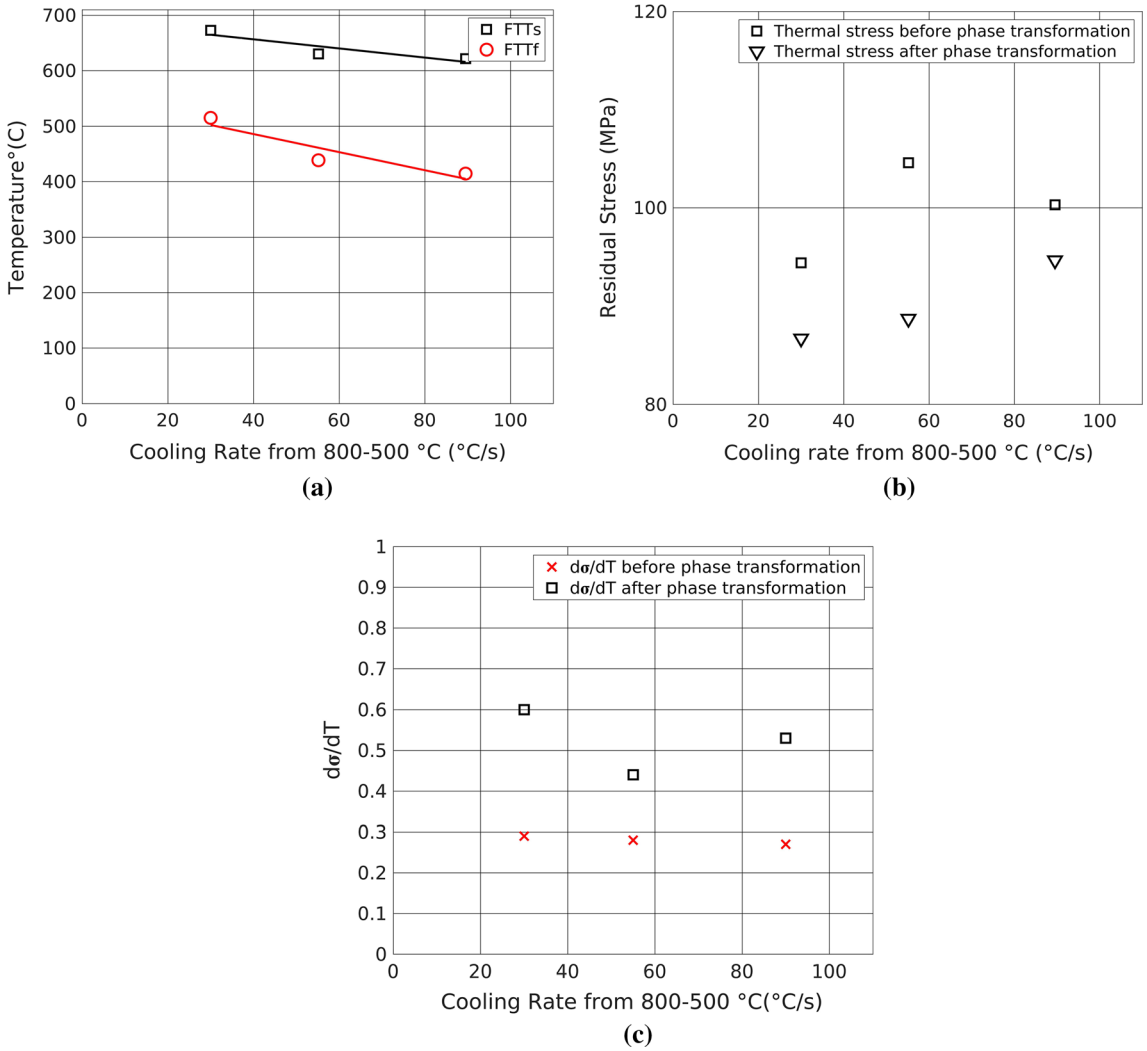

Figure 13 WTSD parameters (Fig. 6) as a function of cooling rate (measured values) for peak temperature of 1100 °C: **a** starting (FFT_s) and finishing (FFT_f) transformation temperatures; **b** thermal stresses before (TS_s) and after (TS_f) phase transformation during cooling; **c** stress–temperature curve ($d\sigma/dT$) before and after phase transformation.

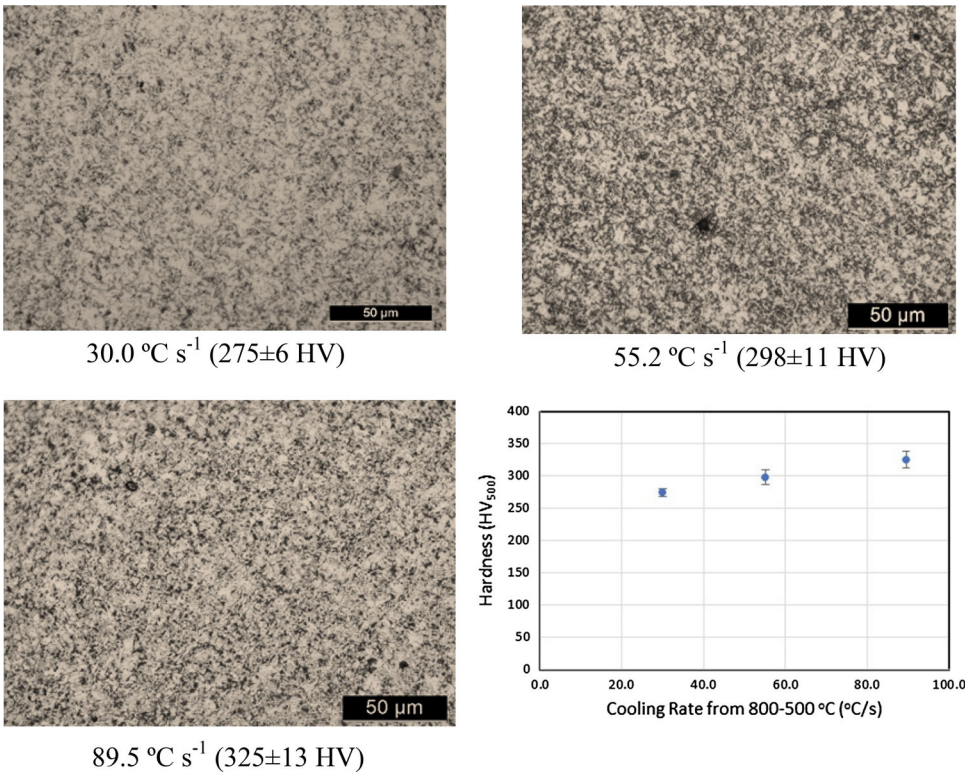

Figure 14 Microstructures of cross sections and respective average hardness (HV_{500}) of simulated specimens as a function of cooling rate (measured values) for peak temperature of 1100 °C.

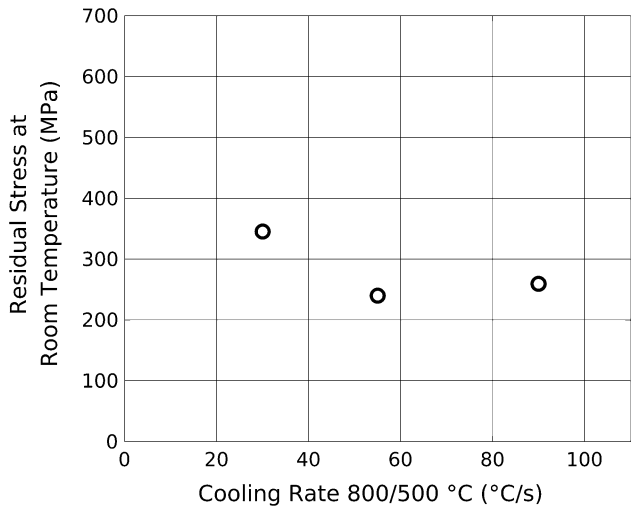

Figure 15 Residual stress-related WTSD parameter (Fig. 6) as a function of cooling rate (measured values) for peak temperature of 1100 °C.

shift. Therefore, the assumption of 900 °C and 700 °C, respectively, for A3 and A1 (considering the composition shown in Table 1 and heating rate shown in Table 2) seems to be acceptable.

As planned in Table 2, for these T_{peak} only 2 nominal values of CR_{8-5} (30 and 90 °C s^{-1}) were assessed. Figures 16 and 17 present the WTSD for peak temperatures of 900 °C and 700 °C, respectively. By comparing these figures with Fig. 12 (T_{peak} of 1100 °C) and Fig. 7 (T_{peak} of 1350 °C), one can initially see that transformation temperatures during heating are again slighter higher, showing a consistent behaviour (naturally no heating transformation for T_{peak} of 700 °C). Another visible difference from comparing the four figures was having no transformation during cooling when T_{peak} was equal to or lower than 900 °C.

Micrographs of cross sections and respective average values of microhardness of these two conditions are shown in Fig. 18. The predominance of martensite and bainite seems to occur only for higher values of CR_{8-5}. Hardness values of conditions with slower CR_{8-5} are only slightly higher than base metal hardness (259 HV ± 11 HV). In addition, hardness at 900 °C or 700 °C assumed similar values. In turn, measurements of length of heated metal volume were not possible also because of low peak temperature reached. Consequently, the effect of under-restriction contraction on RS generation was not directly quantified (but this effect exists and may be a reason for the hardness increase in relation to base metal with no influence of the thermal cycles). In addition, from Fig. 17 it is difficult to distinguish phase

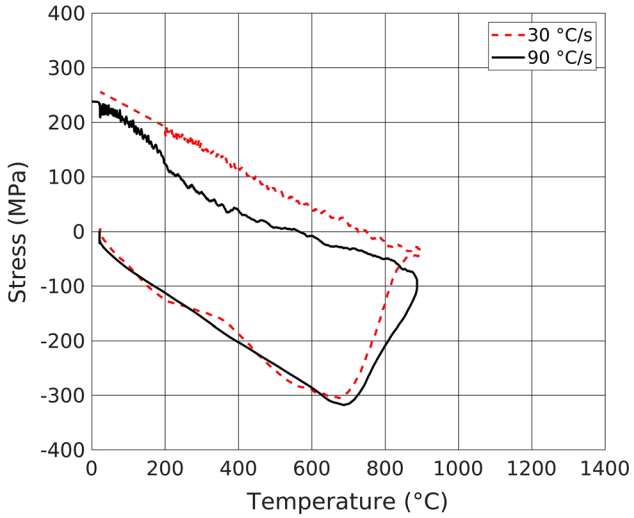

Figure 16 WTSD for different cooling/heating rates having a peak temperature of 900 °C.

transformation. Therefore, the final RS shown in Fig. 19 obtained from WTSD curves as a function of what cooling rate would at first sight represent as the action of under-restriction contraction, proportionally to $CR_{8\text{-}5}$. As such, lower RS (less heating) would be expected than that which occurred. Also, one would expect that the faster the $CR_{8\text{-}5}$, the lower the RS, which cannot be seen in Fig. 19. However, even though not related to expansive phase transformation, a faster cooling rate led to greater hardness at both peak temperatures, inducing lower capacity of

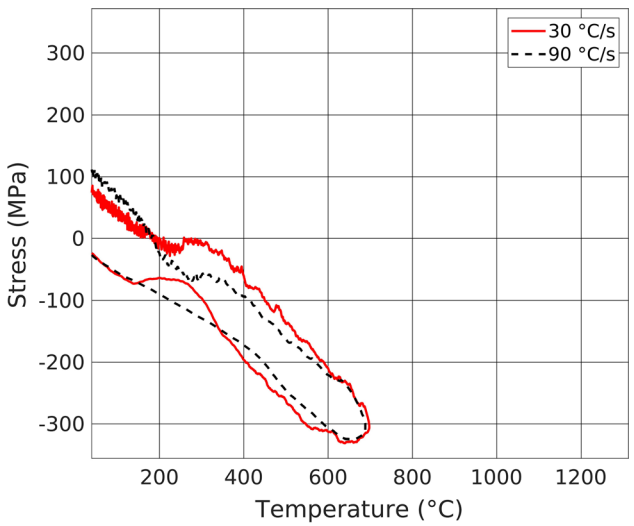

Figure 17 WTSD for different cooling/heating rates having a peak temperature of 700 °C.

the microconstituents to absorb plastic deformation during cooling, thus preventing reducing RS.

General discussion: profile of residual stress

Figure 20 presents the profile of residual stresses (RS) along HAZ for different cooling rates, from which values were taken from WTSD. As seen, trends agree quite well with what is expected for a quenchable steel HAZ, in which the refined grain region would present the highest residual stresses. Results also showed that WTSD was able to present a very realistic balance between the effect of both under-restriction contraction of heated material (welding energy related) and microconstituent expansibility during phase transformation during cooling (material, grain size and cooling rate related). For instance, although from under-restriction contraction of the heated material point of view one should expect higher RS for faster cooling rates, the higher microconstituent expansibility during cooling phase transformation made up for reducing RS for 90 and 55 °C s^{-1}. For this case study (material and thermal cycles), the highest TR was obtained at a cooling rate of 50 °C s^{-1}.

Conclusions

Figure 20 supports, by the coherence of the residual stress distribution at different positions of HAZ and under the effect of different cooling rates, the conclusion that the concept of welding thermal stress diagrams (WTSD) is correct and that the methodology to raise a WTSD by physical simulation is feasible. The proof of this concept carried out with a HSLA steel confirmed that:

(a) Generation of thermal stresses (TS) in a quenchable steel during welding cooling periods is governed by two complex concurrent phenomena, contraction under restriction of heated areas and expansibility of phase transformation from austenitic temperature;

(b) Complexity of concurrent phenomena is enhanced by several facts, such as thermal stress absorption capacity (deformation) of surrounding areas (which in turn depend on

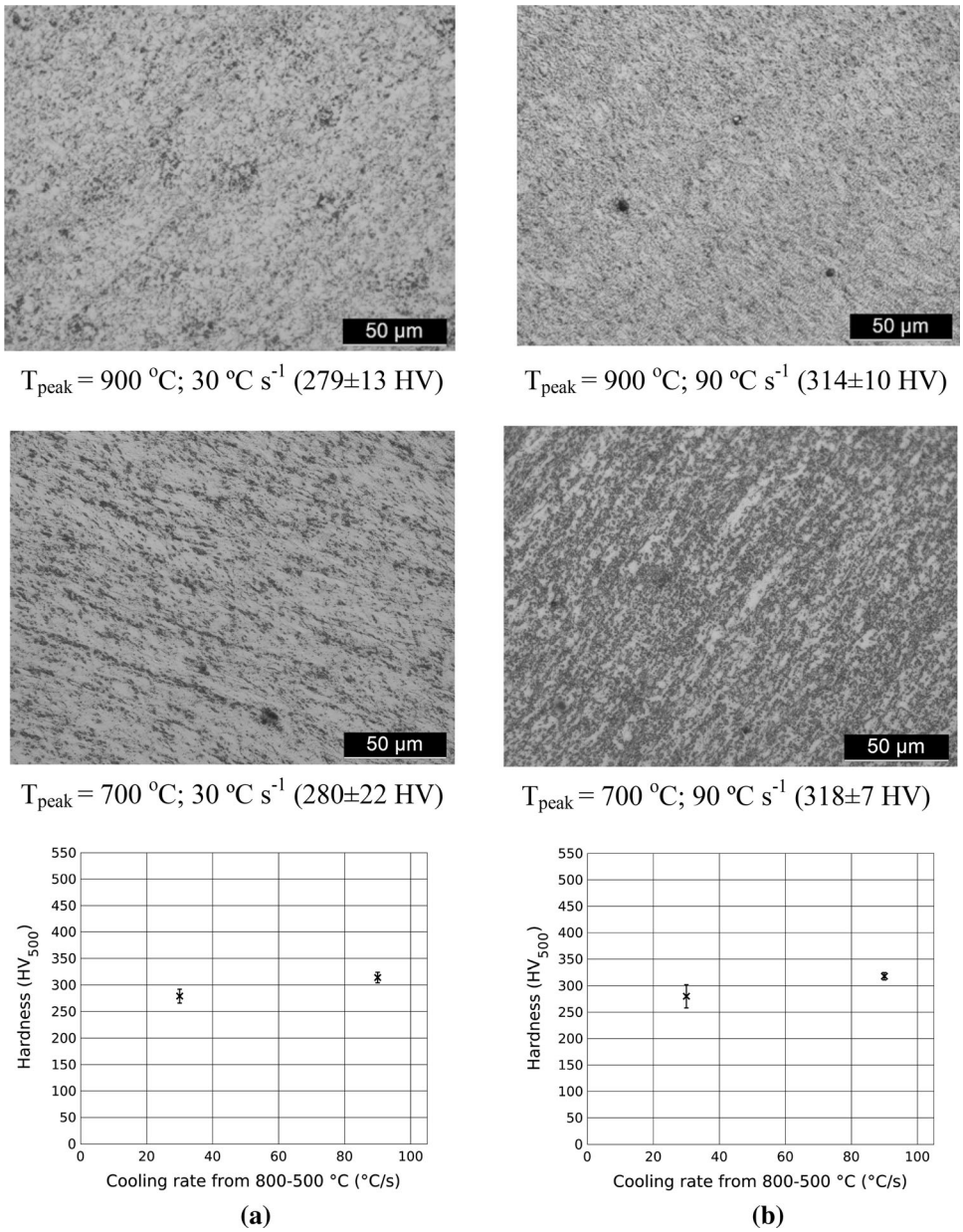

Figure 18 Microstructures of cross sections and respective average hardness (HV_{500}) of simulated specimens as a function of cooling rate (measured values) for: **a** peak temperature of 900 °C; **b** peak temperature of 700 °C.

grain size and microconstituents) and starting and finishing temperatures of expansive phase transformation;

(c) Due to this balance, the highest residual stress (RS) does not necessarily happen either at the slowest cooling rate (corresponding to a high heat input), when heated volume would be expected to be the largest, or at the fastest cooling rate (corresponding to a low heat input), when heated volume would be expected to be smaller, yet with more likelihood of having expansive martensitic transformation and at lower starting and finishing transformation temperatures (with the steel under investigation, the highest RS occurred for an intermediate cooling rate from 800 to 500 °C (CR_{8-5}) of 50 °C s^{-1}, but naturally, this value could be different if materials with different quenchability are studied);

(d) Even so due to this balance, the highest RS may not occur at coarse grain zone due to potential reducing effect of phase transformation (with the steel under investigation, the highest RS occurred at the fine grains region of HAZ (average peak temperature of 1000 °C), regardless CR_{8-5}. However, naturally this region could

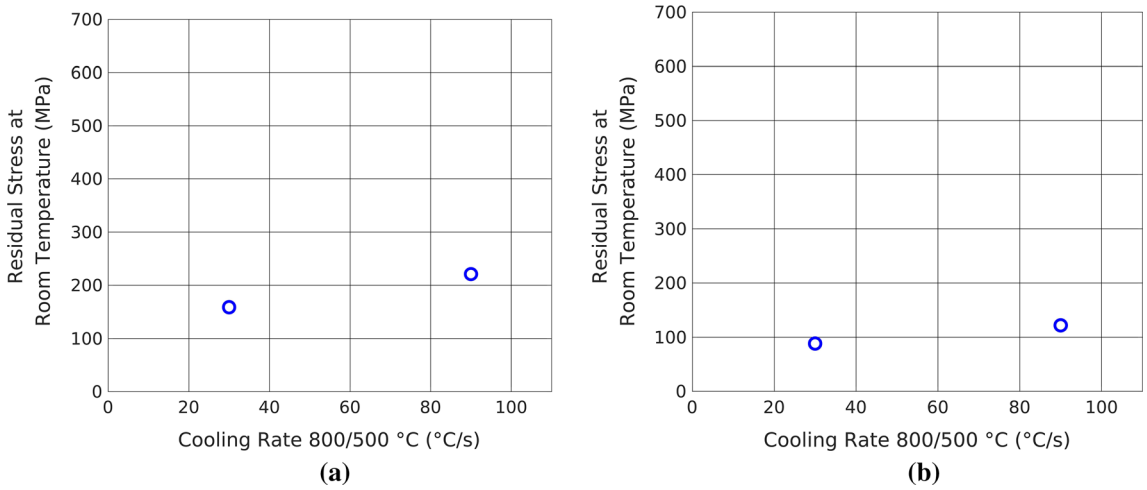

Figure 19 Residual stress-related WTSD parameter (Fig. 6) as a function of cooling rate (measured values) for peak temperature of: **a** 900 °C; **b** 700 °C.

Figure 20 Residual stress profile raised by WTSD approach for the steel in study, as a function of HAZ regions.

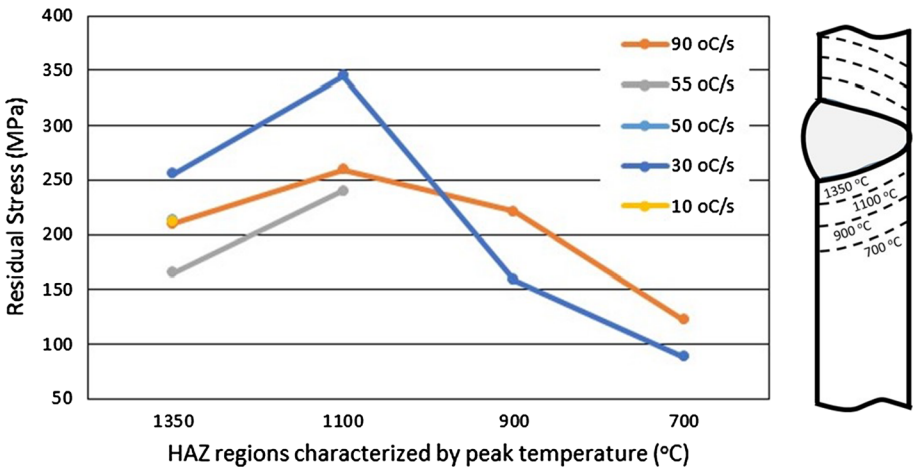

be different if materials with distinct quenchability are studied);

(e) Due to the effect of expansive phase transformation, the increase in TS was hindered during cooling, so that RS values were lower than yield stress resistance of the material under investigation;

(f) Although the quantity of expansive phase transformation (which hinders increase in RS) is minimized or absent in HAZ regions with lower peak temperatures, TS progressively drops not only along HAZ regions away from critical regions due to lower temperature heated volume (contraction under restriction), but even at sub-critical regions there is tensile RS.

In addition, it was also concluded that WTSD by physical simulation allows one to determine the deformation behaviour of material as a function of temperature (stress–temperature curve—$d\sigma/dT$), for different thermal cycles, during heating and cooling periods and that such information can be used as input or calibration in modelling for thermal stress generation in steels. It can also be used as an important tool to understand the role of LTT materials as a means of mitigating residual stresses.

Acknowledgements

The authors would like to thank the Center for Research and Development of Welding Processes (Laprosolda) of the Federal University of Uberlandia and the Brazilian Nanotechnology National

Laboratory—LNNano, for laboratorial infrastructures. The authors also would like to acknowledge financial support provided by the Brazilian National Council for Scientific and Technological Development (CNPq), through Grants Numbers 302863/2016-8 and 149308/2014-0, and from the Minas Gerais State Agency for Research and Development (FAPEMIG), through Project Number TEC—APQ-01992-15.

Author contributions

Andrii Mishchenko's main contributions to this work were related to data curation, formal analysis, investigation, methodology, software, visualization and writing (original draft). Americo Scotti's main contributions to this work were related to conceptualization, funding acquisition, methodology, resources, supervision, validation and writing (review and editing).

Funding

Open access funding provided by University West.

Compliance with ethical standards

Conflicts of interest The authors declare to have no conflicts of interest.

References

[1] Shome M, Mohanty ON (2006) Continuous cooling transformation diagrams applicable to the heat-affected Zone of HSLA-80 and HSLA-100 steels. Metall Mat Trans A 37:2159–2169. https://doi.org/10.1007/BF02586136

[2] Cruz-Crespo A, Araujo DB, Scotti A (2013) Effect of tempering pass on HSLA-80 Steel HAZ microstructures. Weld J 92(10):304s–311s

[3] Scotti A, Li H, Miranda RM (2014) A Round-Robin test with thermal simulation of the welding HAZ to draw CCT diagrams: a need for harmonized procedures and microconstituent terminologies. Soldag Insp 19(3):279–290. https://doi.org/10.1590/0104-9224/SI1903.11

[4] Jones WK, Met, B, Alberry PJ (1978) The Role of Phase Transformations in the Development of Residual Stresses During the Welding of Some Fast Reactor Steels. In: Proceedings of the international conference on ferritic steels for fast reactor steam generators. London: BNES (British Nuclear Energy Society at the Institution of Civil Engineers): pp 471–475.

[5] Scotti A (2016) Five-bar and one-bar models for thermal stress generation in the FZ, HAZ, and BM during arc welding. Weld Int 30(5):329–337. https://doi.org/10.1080/09507116.2015.1096495

[6] Poorhaydari K, Patchett BM, Ivey DG (2005) Estimation of cooling rate in the welding of plates with intermediate thickness. Weld J 84(10):149–155

[7] Kumar R, Ghosh PK, Kumar S (2017) Thermal and metallurgical characteristics of surface modification of AISI 8620 steel produced by TIG arcing process. J Mater Process Technol 240:420–431. https://doi.org/10.1016/j.jmatprotec.2016.10.020

[8] Xu WW, Wang QF, Pan T, Su H, Yang CF (2007) Effect of welding heat input on simulated HAZ microstructure and toughness of A V-N microalloyed steel. J Iron Steel Res Int 14(5):234–239. https://doi.org/10.1016/S1006-706X(08)60085-0

[9] Wang LW, Liu ZY, Cui ZY, Du CW, Wang XH, Li XG (2014) In Situ Corrosion characterization of simulated weld heat affected zone on API X80 pipeline steel. Corros Sci 85:401–410. https://doi.org/10.1016/j.corsci.2014.04.053

[10] Jordan AD, Uwakweh ONC, Maziasz PJ, Reed RW (1999) Weld thermal simulation and its effect upon the microstructure of As-cast FeAl-based materials. Mater Charact 43(4):227–233. https://doi.org/10.1016/S1044-5803(98)00040-0

[11] Ramirez AJ, Brandi SD, Lippold JC (2004) Secondary austenite and chromium nitride precipitation in simulated heat affected zones of duplex stainless steels. J Sci Technol

Join Weld 9(4):301–313. https://doi.org/10.1179/136217104225021715

[12] Rosenthal D (1941) Mathematical theory of heat distribution during welding and cutting. Weld J 20(5):220s–234s

[13] Rykalin NN (1971) Nikolaev AV (1971) welding arc heat flow. Weld World 9(3/4):112–132

[14] Hattingh RJ, Pienaar G (1998) Weld HAZ embrittlement of Nb containing C-Mn steels. Int J Pres Ves Pip 75:661–677. https://doi.org/10.1016/S0308-0161(98)00066-0

[15] Moon J, Kim S-J, Changhee L (2011) Effect of thermo-mechanical cycling on the microstructure and strength of lath martensite in the weld CGHAZ of HSLA steel. Mater Sci Eng A 528:7658–7662. https://doi.org/10.1016/j.msea.2011.06.067

[16] Kumar S, Nath SK, Kumar V (2016) Continuous cooling transformation behavior in the weld coarse grained heat affected zone and mechanical properties of Nb-Microalloyed and HY85 steels. Mater Des 90:177–184. https://doi.org/10.1016/j.matdes.2015.10.071

[17] Zheng L, Song S-H, Yuan ZX (2013) Grain boundary segregation of antimony in heat affected zones during welding thermal cycles for A Cr–Mo low alloy steel. Mater Lett 96:152–154. https://doi.org/10.1016/j.matlet.2013.01.042

[18] Çam G, Özdemir O, Koçak M (2010) Progress in Low Transformation Temperature (LTT) Filler Wires: Review. In: Proceedings of the 63rd annual assembly & international conference of the international institute of welding. Istanbul: [s.n.], pp 759–765

[19] Kannengiesser T, Kromm A (2009) Formation of welding residual stresses in low transformation temperature (LTT) materials. Soldag Insp 14(1):74–81. https://doi.org/10.1590/S0104-92242009000100009

[20] Mishchenko A (2018) A Holistic View of the Generation of Residual Stresses by X-Ray Diffraction in Arc Welding. 200 p. PhD Thesis, Federal University of Uberlândia, Uberlândia, Brazil (**in Portuguese**)

[21] Jorge VL, Gohrs R (2017) Scotti A (2017) Active power measurement in arc welding and its role in heat transfer to the plate. Weld World 61(4):847–856. https://doi.org/10.1007/s40194-017-0470-9

[22] Liskevych O, Scotti A (2015) Determination of the gross heat input in arc welding. J Mater Process Technol 225(2015):139–150. https://doi.org/10.1016/j.jmatprotec.2015.06.005

[23] Hurtig K, Choquet I, Scotti A (2016) Svensson, L-E (2016) A critical analysis of weld heat input measurement through a water-cooled stationary anode calorimeter. J Sci Technol Join Weld 21(5):339–350. https://doi.org/10.1080/13621718.2015.1112945

[24] Zhao S, Wei D, Li R, Zhang L (2014) Effect of cooling rate on phase transformation and microstructure of Nb–Ti microalloyed steel. Mater Trans 55(8):1274–1279. https://doi.org/10.2320/matertrans.M2013395